J. Min. Metall. Sect. B-Metall. 60 (1) (2024) 15 - 31

Journal of Mining and Metallurgy, Section B: Metallurgy

EFFECT OF REGULAR THICKNESSES ON THE MICROSTRUCTURAL AND QUANTITATIVE ANALYSIS FOR A HYPO-EUTECTIC DUCTILE IRON ALLOYED WITH Ni AND V

E. Colin-García [a,*], R.G. Sánchez-Alvarado [a], A. Cruz-Ramírez [b], M.A. Suarez-Rosales [c], L. Portuguez-Pardo [a], J.C. Jiménez-Lugos [a]

[a] Instituto Politécnico Nacional – ESIQIE, Departamento de Ingeniería en Metalurgia y Materiales, Ciudad de México, México

[b] Instituto Politécnico Nacional – UPIIH, Departamento de Formación Profesional Genérica, Hidalgo, México

[c] Universidad Autónoma Metropolitana – UAM-Azcapotzalco, Departamento de Materiales, Ciudad de México, México

(Received 14 November 2023; Accepted 10 January 2024)

Abstract

Ductile iron contains free graphite nodules within the metallic matrix, which generally consists of ferrite and pearlite in the as-cast condition. The casting thicknesses have a great influence on the size, shape, and quantity of the microconstituents of the metallic matrix and the graphite nodules and thus on the mechanical properties. In this study the cooling rate (caused by the casting thicknesses) on the metallic matrix and the nodular characteristics of a low alloyed ductile iron with 0.8 %Ni and 0.15 %V was investigated. The ductile iron was produced in a sandwich process with ladle inoculation. Six plates of different thicknesses, from 4.3 mm to 25.4 mm, were produced in a green sand mold. The microstructural characterization was performed by optical microscopy (OM), scanning electron microscopy (SEM), and the image J software using different quantification methods. The area method to determine the average nodule size and nodular structure provided more reliable results than the perimeter and total particle count methods. The hardness test on the Rockwell C scale was used for the mechanical characterization. The low content of vanadium added to the ductile cast iron had a negligible effect on the solidification pattern, which was mainly due to the graphitizing impact of the nickel and silicon addition. The results of the microstructural characteristics are therefore primarily due to the cooling rate, which is determined by the casting thickness. The thinnest casting section significantly improved the number of nodules (414 Nod/mm^2), sphericity (0.96), and nodularity (96.21 %). In contrast, the thickest casting plate obtained the highest volume fraction of graphite (10.85 %) and the lowest volume fraction of unwanted particles (0.36 %). The high cooling rate in the thinnest casting plate resulted in the highest hardness of 31.56 HRC due to the higher volume fraction of the pearlite (33.7 %) and carbides (4.5 %).

Keywords: *Ductile iron; Thickness; Microstructure; Cooling rate; Quantitative analysis; Nodular characteristics*

1. Introduction

Ductile cast iron or ductile iron (DI), also known as spheroidal or nodular iron, contains free graphite with a spheroidal shape (nodules) within a metallic matrix. This material has high mechanical properties due to the graphite morphology, which prevents the formation or propagation of cracks [1, 2].

The cooling rate and the alloying elements of ductile iron modify the graphite nodules (morphology, quantity, distribution, or size) and the phases or micro-constituents of the metallic matrix [3]. The cooling rate which is dictated by the casting thickness has a substantial impact on the formation of nodules; the formation of 2770 nod/mm^2 for a plate thickness of 1.9 mm [4] has been reported; this is a higher nodule count than those obtained in standard Y-block samples of 25.4 mm with 225 Nod/mm^2 [5]. Thus, the thicknesses in ductile iron castings have been classified as thin-walled ductile iron (TWDI), with casting sections of less than 4 mm [6]. However, some authors point out that the minimum thickness to be considered as TWDI has yet to be established, and it could be considered as 3, 4 or 5 mm as a maximum value limit [6]. Heavy thickness or thick thickness castings consider large dimensional sections as 75 mm [7] or 300 mm [8]. Conventional wall thickness in ductile iron castings are referred to as “regular thickness” of ductile iron in the range between thin and thick walled ductile iron [9].

Corresponding author: ecoling1400@alumno.ipn.mx

https://doi.org/10.2298/JMMB231114002C

The morphology and the amount of free graphite play an essential role in the microstructure and mechanical properties of ductile iron; these can be modified in samples having different thickness castings, such as crankshaft, due to changes in cooling rate; therefore, it is necessary to characterize each thickness. The most common methods used to analyze ductile iron are i) Graphite particles considering number, size, and nodularity; these parameters of free graphite are known as "nodular features" [10] or nodular characteristics [11]. ii) The phases or micro constituents. However, a more specific and comprehensive microstructural analysis in a ductile iron considers more significant number of nodular characteristics such as the nodule count, the total particle count, the nodule size, the interparticle distance, the sphericity, the nodularity, the volume fraction of nodules, the total number of particles, and the unwanted particles together with the phases or micro-constituents of the metal matrix such as pearlite, ferrite, carbides and the ferrite/pearlite ratio.

Two methods are currently used to determine the nodular characteristics. The first is a comparative method in which micrographs are taken at 100X and compared to representative images listed in the ASTM A 247 standard. The second method uses micrographs and specialized software to obtain more accurate results; this method was termed "quantitative analysis," the aim of which is to obtain characteristics of the three-dimensional effect from measurements of two-dimensional objects on polished or etched metallic surfaces [12]. With the advancement of science, the results computed in 2-D can be employed in complex mathematical models that represent suitable results in 3-D [10]; this is a step forward for researchers and science. However, at the industrial level, e.g. in the automotive sector, quantitative analysis in 2-D is still used for the components, as more accurate results can be obtained relatively quickly and without many complications [13, 14].

Quantitative analysis is widely used to characterize ductile iron with different alloying elements [15], the quality of ductile iron before austempering heat treatment [14], the phases obtained after hardening induction as industrial components [16] or to study nodular characteristics in thin or thick thicknesses [6, 8]. Nevertheless, due to the importance of nodular morphology in ductile irons, some investigators focus on a particular nodular characteristic. Riposan I. [17] used two mathematical models according to ISO 945-4-219 and ISO 16112:2017 to assess the nodularity, and concluded that the best nodularity result was obtained with the ISO 945-4-219 model. Sosa A.D. [18] studied the number of residual stress nodules and the distortion of TWDI plates having different metallic matrices, and concluded that residual stress and distortion are highly affected by the number of nodules. Other authors have focused their studies on the effects of alloying elements on the metallic matrix. Colin Garcia E. [19] investigated the addition of nickel in three casting modulus of ductile iron. The results showed that nickel contributed to avoid the formation of iron carbides and to obtain a high amount of pearlite in the metallic matrix with low thicknesses. Sazegaran H. [20] studied the influence of aluminum and copper on the microstructure and morphology of graphite in ductile iron and concluded that increasing these alloying elements increased both the number of nodules and the volume fraction of pearlite and graphite while the nodularity decreased.

On the other hand, vanadium is a carbide stabilizer; its addition to ductile cast iron increases the strength and hardness by increasing the pearlite amount due to the formation of eutectic carbide, which appears as slight white inclusions in the microstructure [14].

With the advancement of characterization techniques, new ways have been discovered to obtain more accurate results in the characterization of graphite and phases in the matrix, such as quantitative 3-D analysis of graphite morphology based on XRD [21] or the analysis of sphericity and spatial distribution of graphite nodules based on morphological tools (mathematical models and imaging software) [22]. Due to its versatility, the quantitative analysis of ductile iron can still be performed using straightforward equations or mathematical models.

Mechanical characterization of ductile iron is mainly performed in Y-block castings to obtain samples as a tensile or compressive test, fatigue, impact, and hardness. However, it is a problem to evaluate different thicknesses in TWDI because the walls are too small to obtain samples for various mechanical tests; on the contrary, for thick thickness castings several samples are required to obtain an accurate result. One way to evaluate the changes in the mechanical properties in ductile iron with different thicknesses is hardness, as it is very versatile and requires only a small section of thickness to evaluate the change in microstructure with respect to the metallic matrix. Rockwell C hardness is commonly used for this purpose.

The hardness of ductile iron is affected by three elements in the chemical composition: carbon, silicon, and phosphorous since these elements are associated with a parameter called carbon equivalent (CE), which modifies the metallic matrix. The relation between the three elements is shown in Equation (1). Ductile irons with CE values below 4.3 % are called hypo-eutectoid ductile iron; those with CE values above 4.3% are called hyper-eutectic, while eutectic ductile irons have a CE of 4.3 % [23].

$$CE = \%C + \left(\frac{1}{3}\right)(\%Si + \%P) \quad (1)$$

Numerous studies on the hyper-eutectic ductile irons can be found in the literature because a high carbon equivalent improves some nodular characteristics such as the nodule count and the nodule size, and modifies the phases, thereby increasing the hardness. However, an adverse effect is that nodules sometimes have excessive nodule size, losing sphericity. In this work the graphite features of a hypo-eutectic ductile iron low alloyed with 0.8 % Ni and 0.15 %V were investigated in detail. It is expected that the nickel addition improves the nodule count and homogenizes the sphericity, while the vanadium increases the hardness of the ductile iron due to the formation of carbides; nevertheless, the nodule count and nodularity of graphite are decreased [19, 24]. In this sense, the study represents an in-depth analysis of the quantitative determination of the main graphite features by applying classical equations. The effect of six regular plate thicknesses (from 4.3 to 25.4 mm) was studied on the nucleation-growth of nodules and phases or micro-constituents and their impact on the hardness.

2. Experimental procedures

2.1. Foundry of castings

A ductile iron alloyed with 0.8 % nickel and 0.15 % vanadium was produced in a coreless induction furnace medium frequency with a capacity of 50 kg. The molten base iron was produced from 35 % cast iron scrap, 30 % low carbon steel (1018), and 35 % pig iron in the temperature range of 1490 – 1520 °C. The metal base was adjusted to obtain the chemical composition by a high carbon riser as recarburizing, FeSi (75 %), high purity nickel, and FeV (75 %). The molten metal was inoculated with 1 % calcifer (75 %Si + 1 %Ca, 0.9 %Al, 1.1 %Ba) in the stream from the coreless induction furnace to the ladle, where it was simultaneously nodulized with 1.5 % MgFeSi agent (45 %Si, 8 %Mg, 3.3 %Ca, 3 % rare earth) in a sandwich process. The treated metal was poured at a temperature of 1450 ºC into green sand molds that were previously made with a model pattern of six plates as shown in Fig. 1a. The molds were shaken out after cooling of 30 minutes. The six plates of the model have the following dimensions: 120 mm in length, 40 cm width and variable thicknesses of 4.3, 8.5, 12.7, 16.9, 21.1, and 25.4 mm. Fig. 1b shows the manufactured plates cut from the feeding system.

The nominal chemical composition of DI was determined using an emission optical spectrograph (ARL Thermo scientific, model 360, 4725-series). The measurement was performed on three different plates to determine the average composition.

2.2. Microstructural characterization

The rough surface of the plates (approximately 1.5 mm) in contact with the molding sand, as shown in Fig. 2a, was rectified to eliminate possible surface defects such as porosity or micro-shrinkage. They were cut along lines A-A' and B-B' as shown in Fig. 2b to obtain microstructural and hardness characterization specimens. The microstructural characterization was performed using Olympus PMG-3 optical microscopy images. In addition, EDS-SEM was used to determine the elements in the carbides, and images were taken in a scanning electron microscope, a JEOL model 6300. For the microstructural analysis, three micrographs were taken 100X magnification for each point of a, b, c, d, and e, as shown in Fig. 2b. The samples were prepared using conventional metallographic procedures: the roughing was performed using abrasive paper grades 180, 220, 320, 400, 600, and 1000, the polishing was carried out with Al_2O_3 powder with a size of 0.3 μm and the chemical etched was performed using two chemical reagents; nital 3% and ammonium persulfate 10 %.

2.3. Quantitative analysis of ductile iron

Quantitative analysis was performed using Image J software with a ratio of 1.11 pixels/microns and micrographs at 100X on polished condition to obtain nodular characteristics such as total particle count, nodule count, nodule size, sphericity, nodularity, interparticle distance, volume fraction of graphite in total particles, graphite of nodules, and unwanted

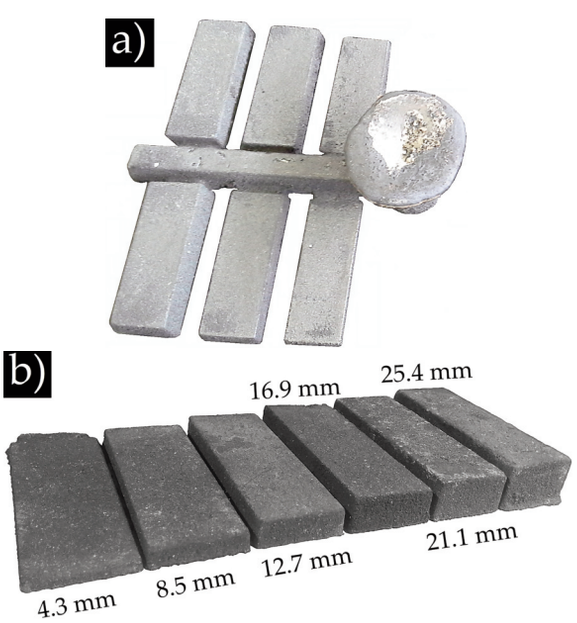

Figure 1. *Model of the plates a) after casting and b) plates cut from 4.3 to 25.4 mm*

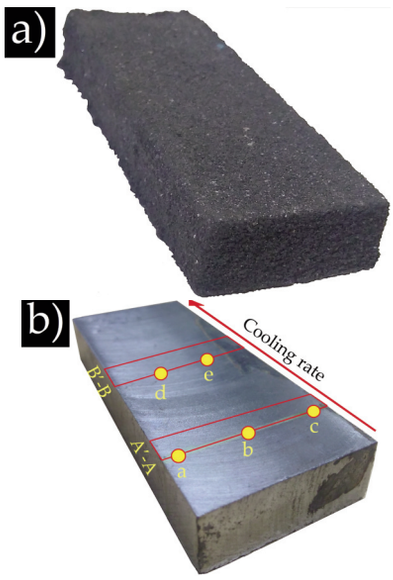

Figure 2. *Plate thickness of 12.7 mm a) surface in contact with green sand, and b) plate rectified*

particles. These results were obtained considering 65 % of sphericity and a minimum diameter size of 10 µm [25], related to a regular thickness of ductile iron. Furthermore, ferrite and pearlite volume fractions were obtained on micrographs under nital-etched conditions, while the volume fraction of carbides was determined with ammonium persulfate under etched conditions.

2.4. Hardness

Rockwell C hardness measurements were obtained with a load of 150 kg and a diamond tip indenter according to ASTM E 18. The indentations were made on polished surface samples in a cross-section through a durometer Wilson 3T TBRB model. The average of 7 measurements and the standard deviation were reported for each plate thickness.

3. Results and discussion

3.1. Chemical composition of ductile iron

The chemical composition of ductile iron alloyed with 0.8 % nickel and 0.15 % vanadium is shown in Table 1. Silicon promotes the formation of ferrite and it can suppress the formation of carbides [26]. In high concentrations, manganese is strongly pearlite-forming, which leads to the formation of carbides in the grain boundaries. In addition, manganese segregation delays the stability of super-cooled austenite and obstructs the graphite nodulizing process [27]. Therefore, a manganese content of less than 0.3% is preferable if the casting has a thin thickness and heat treatment is carried out [28]. The residual magnesium content in ductile irons should be 0.02 - 0.05 % to obtain a correct spheroidal graphite [29]. Nickel is a graphitizing element [19], while vanadium is a carburizing element [30].

The carbon equivalent (CE) was obtained using Equation (1) with the elements listed in Table 1. The CE result was 4.1, which corresponds to hypoeutectic ductile iron. CE is a solid parameter to be considered in ductile iron castings; this indicates the solidification path to determine the first phase that solidifies and changes nodular characteristics. Fatahalla N. [31] reported that hypereutectic DI has a higher nodule count than hypo-eutectic DI. This behavior is due to the fact that in hypereutectic DI the first phase to nucleate and grow is graphite [32].

3.2. Microstructural characterization of ductile iron

Fig. 3 shows the micrographs in the polished condition of the six plates with different thicknesses from 4.3 mm to 25.4 mm are shown in. It can be seen from the micrographs that the number of nodules decreases with increasing thickness, while the size of the nodules increases. The plate thickness of 4.3 mm presented the highest number of graphite nodules and the smallest size, while the plate thickness of 25.4 mm showed the opposite behavior, with the highest nodule size and the lowest nodule count. The six plate thicknesses presented an even distribution of nodules with good nodularity; however, a lower sphericity is evident in larger graphite nodules such as those formed in the 21.1 mm and 25.4 mm thick plates.

Fig. 4 shows that the microstructures of the six plate thicknesses contain graphite nodules embedded in a metallic matrix composed of a mixture of pearlite and ferrite. As the thickness of the plates decreases, the amount of pearlite increases, as can be observed in the plates with the thicknesses of 8.5 mm and 4.3 mm. The higher cooling rate obtained in the small plates favored pearlite formation. On the other hand, slow cooling rates, as recorded in the larger plates with the thicknesses of 12.7 mm - 25.4 mm favored the formation of ferrite.

The ferrite and carbide phases have a similar white tonality within the metal matrix, making it difficult to perform a quantitative analysis with the Image J software to determine the respective amount. Therefore, an etching with 10% ammonium persulfate was performed to darken the metallic matrix,

Table 1. *Chemical composition of ductile iron alloyed with nickel and vanadium (wt%)*

C	Si	Mn	P	S	Mg	Ni	V	Cu	Cr	Mo	Ti	Sn	Pb	Al	As	CE
3.0	3.34	0.35	0.014	0.003	0.03	0.85	0.15	0.12	0.05	0.008	0.006	0.07	0.01	0.02	0.003	4.11

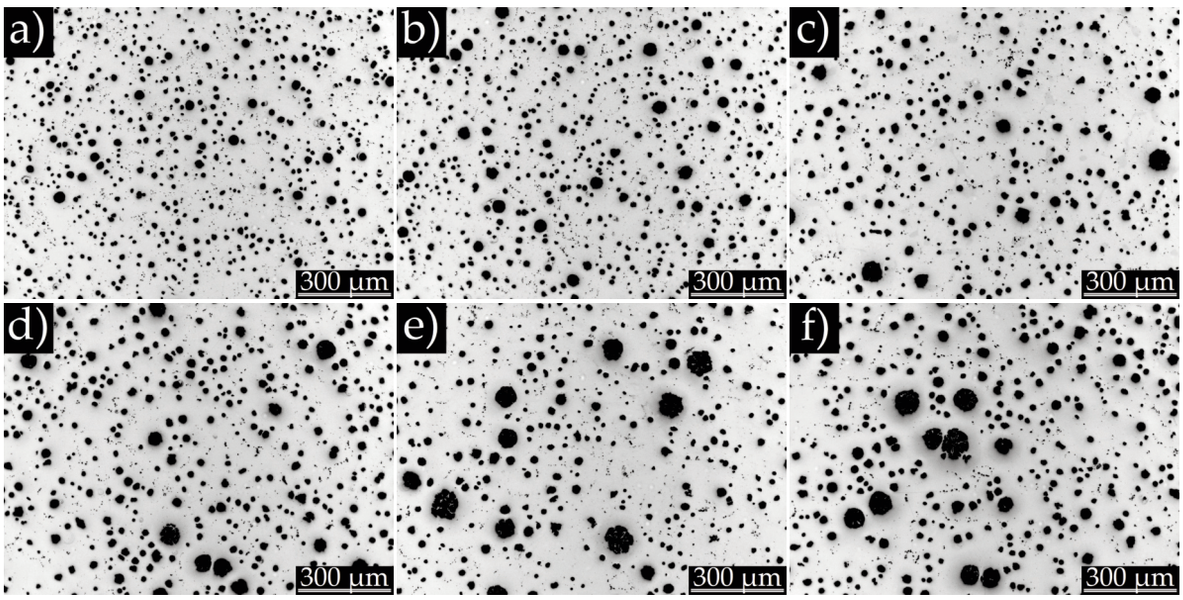

Figure 3. *Micrographs on polished condition for plate thickness a) 4.3, b) 8.5, c) 12.7, d) 16.9, e) 21.1, and f) 25.4 mm*

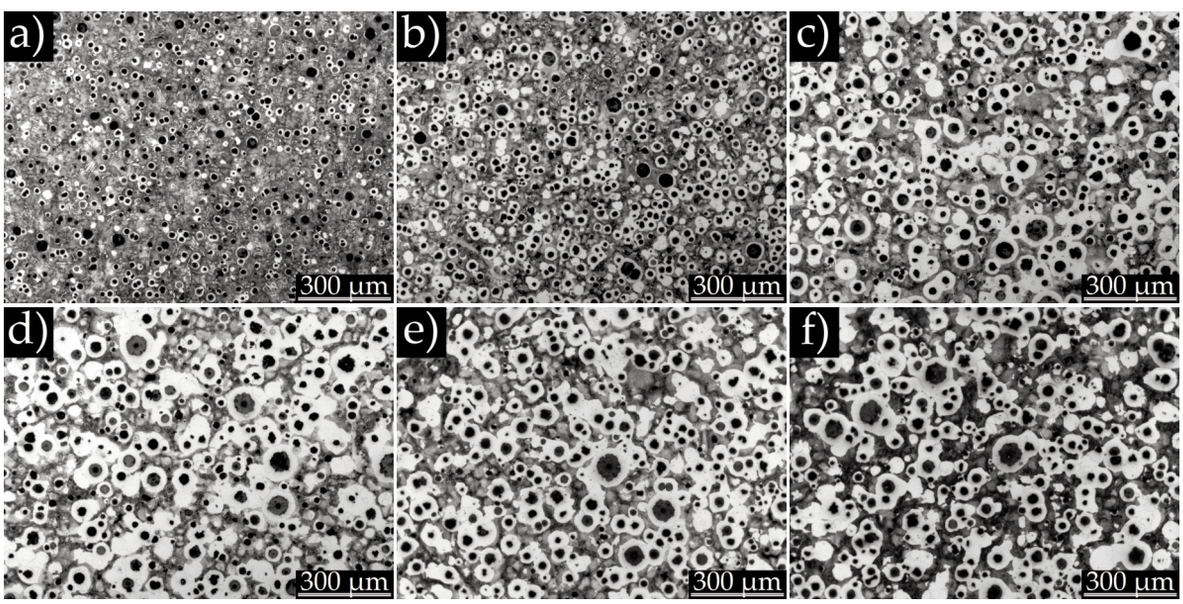

Figure 4. *Micrographs at nital etched condition for plate thickness a) 4.3, b) 8.5, c) 12.7, d) 16.9, e) 21.1 and f) 25.4 mm*

revealing the carbides in a bright white color [33]. Fig. 5 shows the presence of the carbides formed in the six plates of different thicknesses from 4.3 to 25.4 mm. The largest amount of carbides was formed at a plate thickness of 4.3 mm, which decreases up to a plate thickness of 12.7 mm. No carbides were formed at thicker thickness of 16.9 to 25.4 mm.

3.3. Quantitative analysis of ductile iron

3.3.1. Nodule count and total particle count

During the solidification of ductile iron, two types of graphite particles can form; the first one is the graphite nodules, and the second one is irregular graphite shapes such as vermicular or hemispherical particles. Based on this classification, there are two ways to quantify the graphite particles. 1) Nodule count. The number of graphite nodules in a micrograph is expressed as Nod/mm^2. 2) Total particle count. The total number of graphite particles, including irregular graphite shapes and nodules [34], is expressed as Part/mm^2. Identifying the graphite particles is essential because some nodular characteristics are calculated strictly by the nodule count, while others are determined by the total particle count.

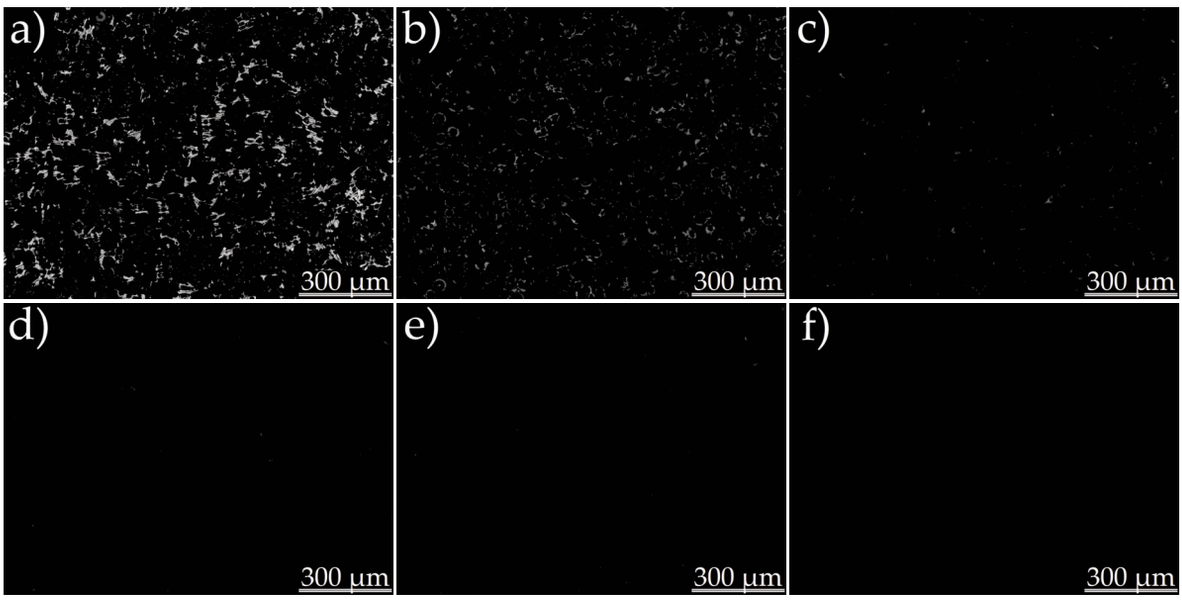

Figure 5. *Micrographs at ammonium persulfate etched for plate thickness a) 4.3, b) 8.5, c) 12.7, d) 16.9, e) 21.1, and f) 25.4 mm*

The nodule count and total particle count for ductile iron with plate thickness of 4.3 to 25.4 mm are shown in Fig. 6. In both cases, the values decrease with increasing plate thickness with the highest values obtained at a plate thickness of 4.3 mm with 414 Nod/mm^2 and 428 Part/mm^2, respectively. It is evident that the total particle count is higher than the nodule count. The distance between the individual points of the curves for the same plate thickness is the number of irregular graphite shapes. In this case, both curves are very close to each other because ductile iron has only a few irregular graphite particles within a larger number of nodules; however, for ductile iron containing a larger number of irregular graphite shapes, the curves can diverge significantly. A high number of nodules is a suitable parameter for the quality of ductile iron. The microstructure becomes finer and reduces the tendency to obtain chill carbides, and this refinement reduces the amount of malformed graphite [35].

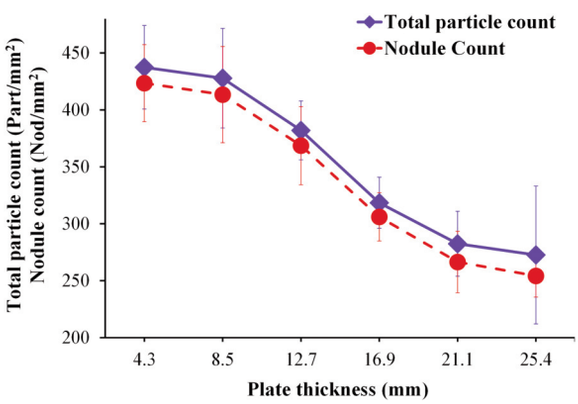

Figure 6. *Nodule count and total particle count for plate thickness from 4.3 to 25.4 mm*

In the hypoeutectic ductile irons, the first growth phase is austenite with a dendritic morphology (austenite proeutectic). The nucleation of the crystals occurs on the mold wall and in the inner melt from which columnar grains are formed. During the formation of austenite, the carbon atoms are expelled into the remaining liquid until a eutectic composition is obtained. From this point, the liquid is transformed into two types of solids, depending on whether the solidification follows the metastable reaction (carbides) or the eutectic one (graphite nodules) [36]. The growth of graphite nodules in the molten metal begins in the particles added in the nodulizing and inoculant agents (magnesium, calcium, or cerium covered by a thin layer of magnesium silicate), which act as heterogeneous nucleation sites [37]. During this stage, many nuclei are formed to precipitate graphite. Initially, these particles do not serve as nucleation sites for graphite because their crystalline structure is not coherent with that of graphite. At the end of the inoculation process, these particles change due to the formation of layers of other silicates and oxides of the inoculating elements. The silicates have the same hexagonal structure as graphite, and thus serve as effective nucleation sites for the growth of graphite nodules [38].

As shown in Fig. 6 various graphite particle counts can be achieved with different solidification cooling rates, which are determined the respective plate thickness. The highest particle and nodule counts were obtained for the plate with a thickness of 4.3 mm, while the lowest nodule count was obtained for the plate with the thickest thicknesses of 25.4 mm.

Górny M. [39] reported a similar behavior, quantifying the highest number of nodules in the small plate of 2 mm, where the highest solidification rates were obtained, and the lowest number of nodules in the plate with a thickness of 15 mm. This behavior can be explained by undercooling. The theory of heterogeneous nucleation shows that for a given substrate, nucleation is instantaneous when a specific undercooling is reached. The number of active nuclei increases at large undercooling caused by high solidification rates because the highest particle and nodule counts were obtained in the thinnest plates [40]. Another critical factor to be considered in the number of graphite nodules and particles are the alloying elements, such as nickel and silicon, which are graphitizing elements that reduce the solubility of carbon in the molten metal and increase the number of ductile iron nodules [41, 42].

3.3.2. Nodule size

The nodule size expresses the diameter of each graphite nodule in microns (µm). The calculation of this nodular characteristic considers a minimum size of 10 µm for regular thicknesses, while for TWDI the minimum size is 5 µm [43]. Strictly speaking, nodule size should not consider irregular graphite shapes such as vermicular, graphite flakes or hemispherical particles (less than 65 % sphericity), as these particles by definition have no diameter.

Two methods can be used to obtain the average size of graphite nodules.1) area and 2) perimeter using the Equations (2) and (3), respectively.

$$NS_{avg} = (2)\left(\sqrt{A\pi^{-1}}\right) \quad (2)$$

$$NS_{avg} = P\pi^{-1} \quad (3)$$

P is the perimeter and A is the area, both for particles considered nodules.

Table 2 shows the values of the average nodule size using the area and perimeter methods for six plates with different thicknesses. Both methods were performed using the Image J software. It is noted that the average nodule size for both methods is very close to each other, with the maximum difference of 0.65 µm in plate thickness of 12.7 mm, which represents less than 1 µm. In this study, the average nodule size is very similar because the tested plates have a constant thickness. However, the authors noted in previous studies that for samples with different thicknesses, such as Cr-alloyed camshafts, the average nodule size varied by up to 7 µm, and was higher in the method of the perimeter.

Although the two methods for determining the average nodule size are reliable, there are some significant differences. Fig. 7 shows a graph with the nodule size distribution of the area and the perimeter methods for plate thickness of 4.3 mm measured in one micrograph corresponding to points a, b, and c shown in Fig. 2b. It is evident that the nodule size by the perimeter method starts at a size of 9 µm (3 nodules), and ends at 31 µm (3 nodules) with a more irregular distribution. In contrast, the area method starts at 10 µm and ends at 30 µm. This behavior means that the perimeter method includes particles below the limit considered as a nodule and obtains a larger nodule size than the area method. Therefore, the area method is used in this study to report the average nodule size, ensuring a minimum size of 10 µm.

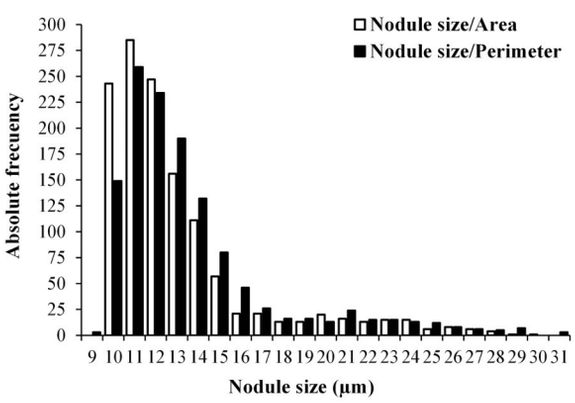

Figure 7. *Distribution of nodule size for plate thickness of 4.3 mm through area and perimeter method*

The nodule size distribution for each plate thickness from 4.3 mm to 25.4 mm is shown in Fig. 8. The plate thickness of 4.3 mm shows the smallest nodule size with a maximum absolute frequency for the size of 10 µm; after the ultimate value, the absolute frequency begins to decrease homogeneously up to a nodule size of 39 µm. As the thickness of the plates increases, the nodule size increases, and the number of nodules decreases. Therefore, the maximum frequency changes from left to right, so that at a plate thickness of 25.4 mm there are fewer small nodules with a larger distribution of nodule size.

Table 2. *Average nodule size by perimeter and area methods for plate thickness from 4.3 to 25.4 mm*

Nodule size Method	4.3 mm	8.5 mm	12.7 mm	16.9 mm	21.1 mm	25.4 mm
Perimeter (µm)	15.09 ± 0.58	17.28 ± 1.11	20.68 ± 1.08	21.98 ± 1.02	22.17 ± 1.64	24.33 ± 1.27
Area (µm)	15.30 ± 0.67	17.42 ± 1.16	20.03 ± 1.44	21.67 ± 1.04	22.41 ± 1.78	24.17 ± 1.37
Difference (µm)	0.21	0.14	0.65	0.31	0.24	0.16

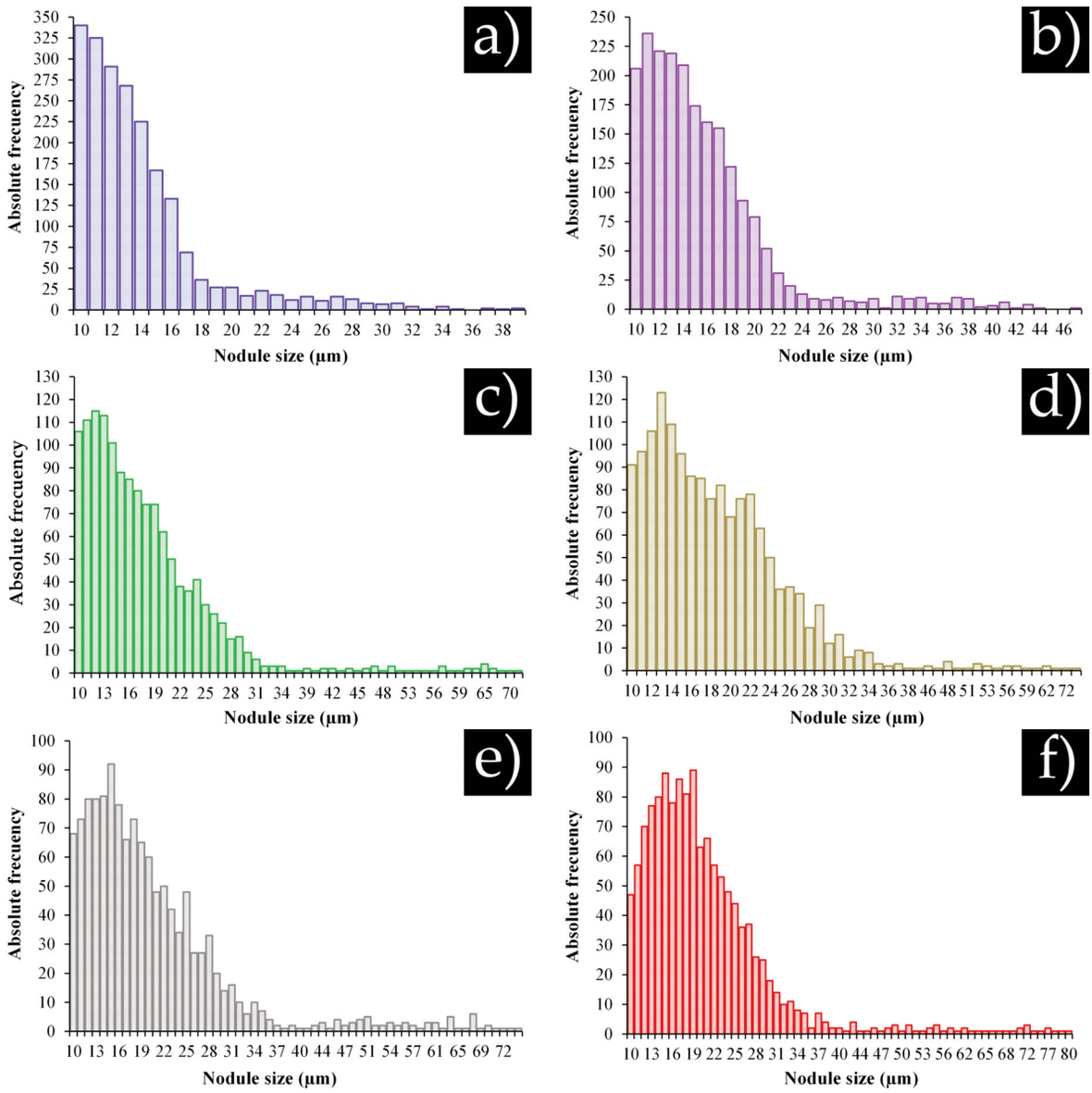

Figure 8. *The Nodule size distribution of plate thickness of a) 4.3, b) 8.5, c) 12.7, d) 16.9, e) 21.1, and f) 25.4 mm*

The liquid-phase carbon precipitates in the form of graphite nodules when the eutectic temperature is reached. The graphite nodules nucleate and grow freely for a short period due to the depletion of carbon atoms in the liquid state. Hence, the austenite nucleates around the graphite nodules due to the low carbon concentration in shell form (austenite surrounds the nodules) and coarse, forming eutectic cells (EC). During eutectic solidification, only the austenite is in contact with the liquid, and carbon diffusion through the austenite shell is the mechanism that controls the nodule growth [44, 45]. Finally, different eutectic cells encounter primary dendrites which form an austenite network with nodules inside and enclose the newly formed nodules [36]. The first nodules formed grow faster than the last, so the liquid decreases until the eutectic solidification ends. The continuous drop in temperature initiates graphitization in the solid state; during this period, the high carbon austenite expels carbon atoms and continues its diffusion into pre-existing graphite nodules until the austenite acquires a eutectoid composition [44]. As already mentioned, the nodule size is affected by the cooling rate, which is determined by the thickness of the plates during solidification. At low plate thicknesses such as 4.3 and 8.5 mm, where the solidification and graphitization occurred most rapidly, the nodules presented a smaller size distribution than at higher plate thicknesses (21.1 and 5.4 mm). Another essential factor is that the

addition of Ni close to 0.8% refines the size of the graphite nodule, and their distribution in the microstructure is more homogeneous [19].

3.3.3. Interparticle distance

The nodule count and the average nodule size are related by a parameter known as the interparticle spacing (λ_G); this nodular characteristic represents the carbon diffusion distance. It should be noted that the average nodule size should not consider the irregular shapes of graphite, as by definition they have no diameter. The interparticle distance is obtained using Equation (4) [25].

$$\lambda_G = (55.4)\left(\frac{NS_{avg}}{Nodule\ count}\right)^{\frac{1}{3}} \quad (4)$$

NS_{avg} is the average nodule size in μm, and nodule count is expressed as Nod/mm^2.

The interparticle spacing measured on plates of different thicknesses from 4.3 to 25.4 μm is shown in Fig. 9. It can be seen that the larger the nodules and the smaller number of nodules, the greater the distance between the particles. The shortest interparticle spacing (18.23 μm) was obtained at a plate thickness of 4.3 mm due to the high cooling rate, while the longest value of 25.33 μm was obtained at a plate thickness of 25.4 mm due to the low cooling rate.

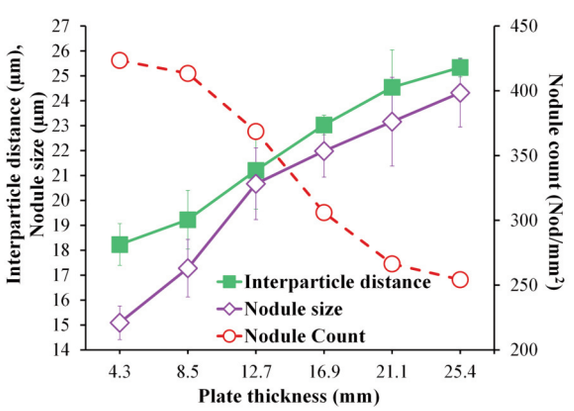

Figure 9. *Interparticle distance for plate thickness from 4.3 to 25.4 mm*

3.3.4. Sphericity and nodularity

Sphericity and nodularity can sometimes be confused; however, both have different meanings. Sphericity refers to the roundness of the nodules in a range of 0.65 to 1.0. These parameters were described by Ruxunda R.E. [25] according to a convention widely used in industrial companies (Image pro-plus, Omnimet Enterprise Handbook, and UTHSCSA Image tool Handbook). The lower limit refers to the minimum roundness accepted to be considered as a nodule, while the higher limit refers to a perfect circle. Sometimes, the accepted minimum sphericity varies [17], and some researchers reported this characteristic as % [46]. The sphericity for this research was obtained using the perimeter and area by the sphericity shape factor shown in Equation (5) [47]. However, there are other equations to obtain this nodular characteristic [48]

$$SSF = \frac{4 \cdot \Pi \cdot Area}{(Perimeter)^2} \quad (5)$$

Nodularity represents the percentage ratio for acceptable particles area (graphite of nodule count) to graphite of acceptable plus unacceptable particles area (total particle count) expressed as a %. Equation (6) [25] shows the standard model used. Nevertheless, sometimes nodularity is also expressed as a percentage of nodule count and total particle count according to Equation (7) [49] or using other mathematical models listed in ISO standards [17].

$$\%Nod = \left(\frac{Area\ of\ nodule\ count}{Area\ of\ total\ particles\ count}\right) \cdot 100 \quad (6)$$

$$\%Nod = \left(\frac{Nodule\ count}{Total\ particles\ count}\right) \cdot 100 \quad (7)$$

Fig. 10 shows that the sphericity decreases with increasing plate thickness, obtaining values of 0.9 to 0.86 for plate thicknesses of 4.3 mm and 25.4 mm, respectively. The higher cooling rate imposed by small thicknesses such as 4.3 mm helps to improve the sphericity close to 1.0, while at larger thicknesses, the graphite nodules are far from being a perfect circle in the trials developed with the same amount and type of nodulizer agent.

As sphericity decreases, nodularity decreases similarly as these nodular characteristics are strongly related. The nodularity decreases with two methods computed: area and count. The nodularity–area values in a range of 96.2 to 87.5 were lower than the nodularity–-count in a range of 96.81 to 93.25 % for a plate thickness of 4.3 to 25.4 mm, respectively. The different size distribution of the graphite particles [45]; as the plate thickness increases, some particles are larger, and consequently, the area increases, and the nodularity area decreases [11]. The sphericity and nodularity values obtained in this research are similar to those reported by Bojarro J.M. [49] for ductile iron with different CE and thicknesses ranging from 1.5 to 38.1 mm. However, Tomaran S. [50] reported that nodularity by the counting method is slightly higher than by the area method for three grades of ductile iron.

The reduction in plate thickness decreases the average nodule size and improves the sphericity and nodularity [51]. This behavior is attributed to

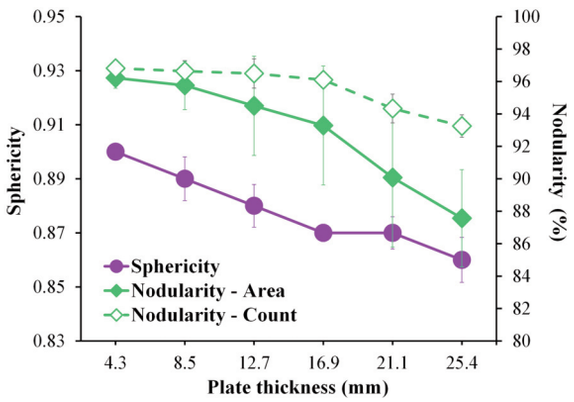

Figure 10. *Sphericity and nodularity for plate thickness from 4.3 to 25.4 mm*

magnesium, rare earth, and the high cooling rate caused by the thickness.

During the production of ductile iron, rare earth, and magnesium are added in the molten metal in the modification stage (in this case, the sandwich technique), generally in the range of 0.03 - 0.05 % to obtain graphite nodules. Anti-spheroidizing elements such as Ti, Bi, Zr, P, N, O, and S are surface-active elements that reduce the surface tension between graphite and liquid. The main surface-active elements, such as O and S, cause changes in the direction of the graphite growth on the A axis, resulting in an irregular graphite shape. The function of Mg and RE is to neutralize the two surface-active elements to obtain the growth of carbon in the Axis C and obtain a spherical shape [52].

During the solidification, the austenite dendrites interact with eutectic cells. Hence, the austenite thickness increases and nodules grow. The uniformity of austenite thickness increases as the time increases during the eutectic temperature, resulting in an uneven supply of atoms for nodular graphite in all directions [53]. Hence, in small plate thicknesses for 4.3 and 8.5 mm, the solidification and graphitization proceed very rapidly so that the initial high nodular formation is somewhat lost. Furthermore, graphite nodules increase in size during the solid state, and nodularity decreases due to the uneven diffusion of the carbon atoms [53]. The final shape of the graphite depends mainly on the rate at which the austenite coats the nodules. This rate depends on the cooling of the casting and is influenced by the amount of magnesium [44]. Therefore, a small thickness requires less magnesium to form nodules, while a larger nodule requires more magnesium. The alloying elements also influence sphericity and nodularity. The addition of vanadium impairs nodularity and promotes the formation of chunky graphite during casting with long solidification times [54]. At the same time, nickel improves sphericity and nodularity [19].

3.3.5. Graphite of nodules, graphite of total particles and undesirable particles

Sometimes, the terms surface fraction and area fraction, among others, are used to describe the amount of phase in a micrograph. Volume fraction is a widely used term that is technically correct because the results are determined by the number of picture elements or "pixels" in stereography or quantitative metallography. Volume, area, line, and point are related by equality; VV = AA = LL = PP expressed as % [12, 55].

The volume fraction for graphite of nodules refers to the amount of graphite contained only in the nodules (sphericity and nodule size greater than 65 % and 10 μm, respectively). The total particle graphite includes irregular graphite shapes (higher than 10) and graphite nodules.

The volume fraction of the graphite of the nodules and the graphite of total particles for plate thickness from 4.3 to 25.4 mm are shown in Fig. 11. With increasing thickness, the volume fraction of graphite increases from 6.31 to 10.85 % and from 6.55 to 11.24 %, for nodule count and particle count, respectively. The gap between the individual points in the curve is the area of irregular graphite shapes.

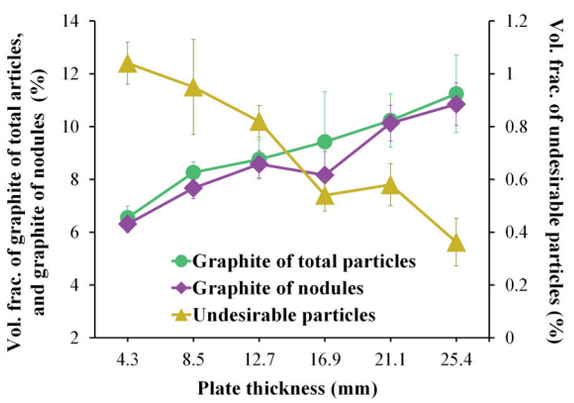

Figure 11. *The volume fraction of graphite nodules, graphite total particles, and undesirable particles for plate thickness from 4.3 to 25.4 mm*

Hypo-eutectic DI generally has a low volume fraction of graphite for nodules and total particles. The growth of graphite shapes (nodules or irregular shapes) increases the volume fraction; this depends on four stages: i) from the liquid, ii) during eutectic transformation, iii) during cooling eutectoid temperature and iv) during eutectoid transformation.

At the beginning of the solidification, austenite and graphite grow separately (separated eutectic), resulting in graphite particles that are in contact with the molten metal. At this point, the austenite dendrites grow, and the carbon is ejected into the interdendritic liquid increasing the viscosity and restricting the

movement of the atoms.

After a certain amount of solid content has formed, dendrite coherence and graphite austenite interaction begin [56]. The graphite phase is then enveloped by a solid austenite shell; the carbon atoms ejected from the austenite diffuse onto the surface of the nodules and irregular shapes and increase the volume fraction of graphite. In plate thicknesses of 21.1 and 25.4 mm, the cooling rate is low, which prolongs the graphitization time and results in a higher volume fraction of graphite and graphite nodules, while graphitization is very short at a plate thickness of 4.3 mm resulting in as a consequence, only a small volume fraction.

The discarded particles computed during the volume fraction of graphite with a maximum size of 10 µm are usually porosity, non-metallic inclusions, pitting [22], micro-shrinkage, and small nodules; these are considered in the volume fraction of unwanted particles. This characteristic is not always analyzed due to the low volume fraction of ductile iron. However, it is essential when applying austempering to DI, as the proportion of porosity and micro-shrinkage should not exceed 1.0 % and the proportion of carbides and non-inclusions should not exceed 0.5 % [57].

The volume fraction of unwanted particles of ductile iron for plate thicknesses from 4.3 to 25.4 mm is shown in Fig. 11. The maximum number of unwanted particles is found in the plate thickness of 4.3 mm (1.04 %), which decreases with increasing thickness up to a plate thickness of 25.4 mm (0.36 %). This behavior is attributed to solid-state graphitization, during which the carbon atoms are ejected from the austenite. At this stage, only carbon atoms close to the surface of the nodules could diffuse to them. At a plate thickness of 4.3 mm, the fast-cooling rate was able to limit the diffusion of carbon atoms from the austenite to the graphite nodules, and then, these atoms nucleated in the form of nodules with an average size of less than 10 µm at the grain boundary of the austenite [53].

On the other hand, with having a greater plate thickness of 25.4 mm, the diffusion time is longer so that the atoms diffuse to the graphite nodules and nucleation at the grain boundaries is avoided, thus reducing unwanted particles. These unwanted particles which are smaller than 10 µm (shown in the red circles) can be seen in Fig. 12 for plate thicknesses of 4.3 and 25.4 mm. The most significant amount of graphite particles was found in the plate thickness of 4.3 mm, which decreases up to the plate thickness of 25.4 mm. In addition, the most considerable volume fraction is attributed to small nodules and irregular graphite shapes.

3.3.6. Ferrite and pearlite

During the graphitization state, the austenite expels carbon until it reaches the eutectoid composition so that the decomposition of the austenite

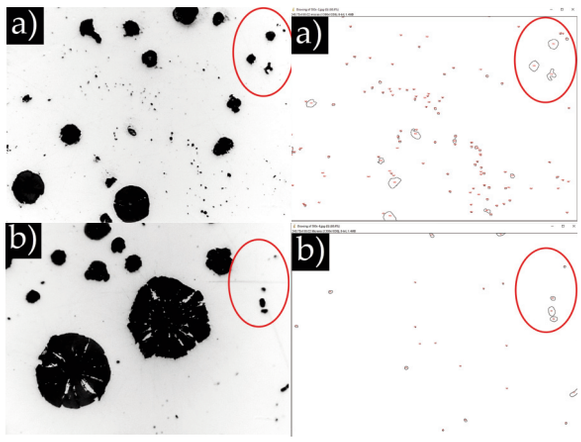

Figure 12. *Graphite nodule size less than 10 µm for thickness a) 4.3 and b) 25.4 mm on polish condition analysed with Image J software*

can lead to the formation of the ferrite phase if the stable reaction occurs (ferritic reaction) or the formation of ferrite and pearlite if the metastable reaction occurs (pearlitic reaction). In addition to the cooling rate and the alloying elements, the eutectoid transformation also depends on the competition between stable and metastable reactions [58].

Fig. 13 shows the volume fraction of ferrite, pearlite, and carbides in the six plates of different thicknesses. The volume fraction of ferrite increased with the increasing thickness of the plates, reaching the highest value (53.68%) at a plate thickness of 25.4 mm.

Ferrite is a phase formed during slow cooling; austenite continues to eject carbon atoms into nodules as the temperature decreases. Ferrite usually nucleates at the nodule/austenite interface and grows symmetrically around the nodules, forming a halo. As the halo grows, the remaining austenite continues to eject carbon atoms to diffuse through the ferrite halo (ferrite reaction), which is thicker [59]. The cooling rate decreases as the plate thickness

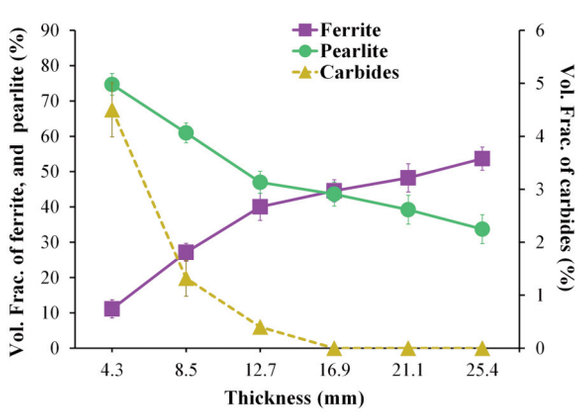

Figure 13. *The volume fraction of phases and micro-constituents for ductile iron from thickness 4.3 to 25.4 mm*

increases to 25.4 mm; the carbon diffusion time increases, resulting in larger amounts of ferrite in the matrix [40], which leads to a decrease in pearlite [60].

Pearlite behaves differently from ferrite. The volume fraction of pearlite increases as the casting plate decreases, obtaining the highest value (74.67 %) at a plate thickness of 4.3 mm. When the ferrite halo is large enough, the diffusion of the carbon atoms through the ferrite gradually decreases. Hence, the temperature drop becomes low enough to nucleate the pearlite (pearlitic reaction).

The preferred nucleation site for the pearlite is the austenite/ferrite interface due to the carbon content in the austenite. However, pearlite grows faster than ferrite due to the cooperative (coupled) growth of cementite and ferrite [59]. When the thickness is reduced to a plate thickness of 4.3 mm, the cooling rate increases the volume fraction of pearlite [40], and as a result, this micro-constituent can nucleate at the austenite grain boundaries or the graphite/austenite interface.

3.3.7. Ferrite/Pearlite ratio

The volume fractions of ferrite and pearlite are of great importance for mechanical properties of ductile iron and are related to each other by the ferrite/pearlite ratio, which can be changed by the cooling rate.

Table 3 shows the volume fraction of ferrite and pearlite and the ferrite/pearlite ratio for ductile iron obtained in the six plates with different thicknesses from 4.3 mm to 25.4 mm. The plates with a thickness of 4.3 mm to 12.7 mm, had a ratio less than 1.0 and consists mainly of a pearlitic matrix, which increases the hardness and strength of the ductile iron.

If the ratio is higher than 1.0, as with a plate thickness of 21.1 to 25.4 mm, ferrite is the predominant phase, so that ductility and toughness increase.

A ferrite/pearlite ratio of 1.02 was determined for the 16.9 mm casting plate. With this ratio an adequate balance between ferrite and pearlite and a good combination of mechanical properties can be achieved.

The behavior of the ferrite/pearlite ratio obtained in this research is similar to that reported by Gonzaga R.A. [61], who reported that the as-cast DI having a 30/70 ratio presents higher hardness than a 60/40 ratio.

3.3.8. Carbides

The volume fraction of carbides for a plate thickness of 4.3 to 25.4 mm is shown in Fig. 13. The amount of primary carbides (formed during solidification) increases as the plate thickness decreases. In this case, the plate thickness of 4.23, 8.46, and 12.6 mm presented carbides, with the highest volume fraction (4.5%) being reached at the plate thickness of 4.3 mm. The carbides were mainly concentrated in the center of the plates at points b, d, and e, as shown in Fig. 2b. Only a minimal amount of carbides was found near the perimeter.

The formation of carbides is attributed to different factors such as [62]; high cooling rate during solidification, carbide-forming elements during the melting step, low CE, low Si content, inadequate or poor inoculation, excessive magnesium content, and high overheating.

In the case of small thicknesses plates where high cooling rates are required, the solidification of ductile iron can occur entirely or partially according to the metastable phase diagram, causing the transformation of the melt into ledeburite [63]. In addition, the carbide content is increased by adding carburizing elements. During solidification, reverse cooling can occur, i.e., segregation of carbide-forming elements such as manganese, vanadium, chromium, molybdenum, or titanium, which increases the concentration of these elements in the remaining liquid to be solidified and promotes carbide formation. The formation of carbides is aided by increasing the concentration of these elements [64]. Although the morphology of carbides is irregular and complex, two distinctive forms can be identified: plate and ledeburite forms [63].

A scanning electron microscope (SEM) was employed to determine the elements inside the carbide plates and the ledeburitics. Fig. 14 shows a SEM micrograph and its punctual analysis in carbides. Fig. 14a shows carbide plates and regions of transformed ledeburite. Fig. 14b shows two points with a chemical composition; this presents a homogeneous distribution and similar main elements, e.g. carbide formation, such as V, Mn, and C.

The addition of nickel and silicon elements together with a low cooling rate prevents carbide formation in plate thickness of 16.9, 21.1, to 25.4 mm. Silicon delays carbide formation [41]. Nickel shows a positive effect on solidification due to the reduction of

Table 3. *Ferrite/pearlite ratio for plate thickness from 4.3 to 25.4 mm*

Characteristic	4.3 mm	8.5 mm	12.7 mm	16.9 mm	21.1 mm	25.4 mm
Ferrite	11.13	27.16	40.04	44.57	48.22	53.68
Pearlite	74.67	60.95	46.97	43.6	32.9	33.7
Ferrite/pearlite ratio	0.15	0.44	0.85	1.02	1.23	1.60

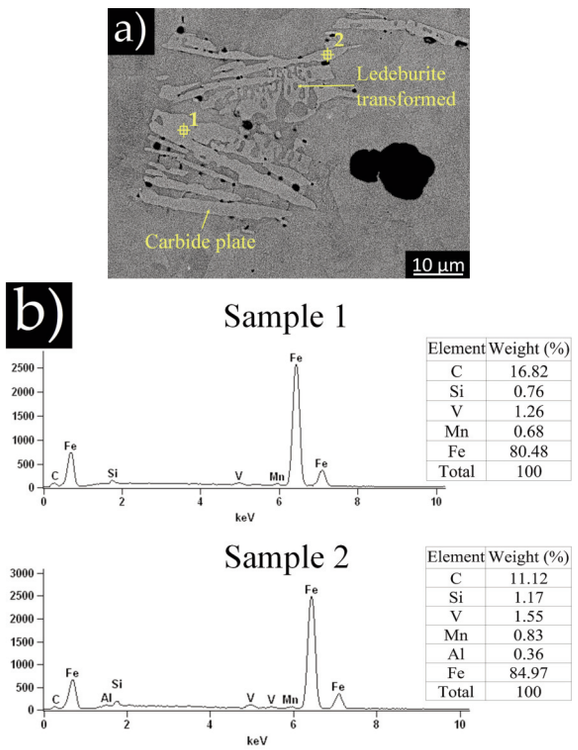

Figure 14. *a) SEM micrograph and b) Punctual X-ray microanalysis of the ductile iron*

carbon content in the eutectic; the interval between the γ-graphite and γ-Fe_3C transformation is increased, which suppresses carbide formation, and therefore nickel prevents a cooling tendency [65].

It has been reported [64] that the addition of vanadium for contents higher than 0.2 % to ductile iron affects the nodule count and nodularity due to carbide formation. However, the low content of vanadium added to the ductile cast iron had a negligible effect on the solidification pattern, which was mainly due to the graphitizer impact of the nickel and silicon addition. The graphite features, and the phase results obtained are related to the effect of the cooling rate, which is dictated by the different thicknesses evaluated.

3.4. Hardness of ductile iron

The hardness values on the Rockwell C scale for ductile iron at plate thickness 4.3 to 25.4 mm are shown in Fig. 15. The hardness increases as the plate thickness decreases. This behavior depends on the phases and micro-constituents within the metallic matrix. These result from the cooling rate which is determined by the thickness during the solidification. As expected, low values of the ferrite/pearlite ratio exhibit higher hardness, such as plate thickness of 4.3 to 12.7 mm, while higher values of the pearlite/ferrite ratio exhibit a low hardness, such as thicknesses of 21.1 and 25.4 mm.

The correct balance of the ferrite/pearlite ratio with a hardness of 19.83 HRC was achieved at a plate thickness of 16.9 mm. The maximum hardness (31.56 HRC) was obtained in the plate thickness of 4.3 mm, which contains the highest volume fraction of pearlite and carbides. It has been reported that the hardness is increased by addition of the carburizing elements such as vanadium or chromium as both contribute to obtaining a higher volume fraction of carbides [24, 66].

On the other hand, the lowest hardness (17.33 HRC) was found in plate thickness of 25.4 mm, which was attributed to the highest volume fraction of ferrite and graphite, both of which are considered soft phases in ductile iron [67]. The results on hardness and its behavior when varying the thickness of the plates are similar to those reported by Guzel E. [68], who worked with plates thicknesses ranging of 12.7 to 76.2 mm.

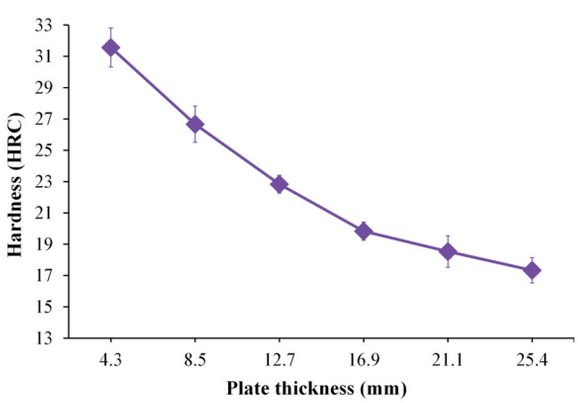

Figure 15. *Rockwell C hardness for plate thickness from 4.3 to 25.4 mm*

It must be mentioned that the accuracy of the results depends on the region analyzed. Therefore, a representative area of the ductile iron sample must be considered in order to obtain reliable results during the measurements of the phases or micro-constituents and nodular characteristics, to obtain the maximum possible data information, and to obtain a correct distribution of the results [55].

Another source of error in the quantification is obtaining incorrect micrographs due to incorrect metallographic preparation of the sample. Thus, adequate metallographic procedures must be applied [69] to obtain high-quality micrographs that increase the accuracy of quantification.

4. Conclusions

The nodular characteristics, phases, or micro-constituents and their relation with the cooling rate imposed by different casting thicknesses were

analyzed in detail in a hypo-eutectic ductile iron alloyed with 0.8 % Ni and 0.15 % V. The results are summarized as follows:

1. The cooling rate imposed by different thicknesses casting strongly changes the nodular characteristics, phases, micro-constituents, and hardness.

2. The area method for determining the average nodule size and nodularity provides more reliable results than the perimeter and total particle count methods.

3. The nodular features of nodule count, sphericity, and nodularity are improved when the casting thickness is decreased. With a casting plate of 4.3 mm the highest nodule count of 414 Nod/mm^2, a sphericity of 0.96 and nodularity of 96.21 % can be achieved. In contrast, the highest volume fraction of graphite and the lowest volume fraction of unwanted particles were achieved with the thickest casting plate.

4. The low content of vanadium added to the ductile cast iron had a negligible effect on the solidification pattern, which was mainly due to the graphitizer effect of the nickel and silicon addition.

5. The higher volume fraction of carbides was achieved in the thinner casting plate due to the high cooling rate during solidification. Carbide formation was suppressed in the casting plate thicknesses of 16.9 to 25.4 mm by a reduction in the cooling rate and the effect of the nickel and silicon addition.

6. The highest hardness of 31.56 HRC was achieved at a casting plate thickness of 4.3 mm due to the higher contents of the volume fraction of pearlite and carbides.

Acknowledgments

The authors wish to thank the Institutions CONAHCYT, SNI, COFAA, and SIP-Instituto Politécnico Nacional for their permanent assistance to the Process Metallurgy Group at ESIQIE-Metallurgy and Materials Department.

Author Contributions

Visualization, Software, and Writing - original draft, E. Colin-García; Data curation, E. Colin-García, M.A. Suarez-Rosales & R.G. Sanchez-Alvarado; Formal analysis, E. Colin-García & A. Cruz-Ramírez; Investigation, Eduardo Colin García & J.C. Jiménez-Lugos; Methodology, E. Colin-García & L. Portuguez-Pardo; Writing – review & editing, E. Colin-García, A. Cruz-Ramírez M.A. & Suarez-Rosales.

Data Availability Statement

Data will be made available on request.

Conflicts of Interest

The authors declare no conflict of interest.

References

[1] T.J. Marrow, H. Çetinel, Short fatigue cracks in austempered ductile iron (ADI), Fatigue & Fracture of Engineering Materials & Structures, 23 (2000) 425-434. https://doi.org/10.1046/j.1460-2695.2000.00295.x

[2] M.A. Neri, C. Carreño, Effect of copper content on the microstructure and mechanical properties of a modified nodular iron, Materials Characterization, 51 (4) (2003) 219-224. https://doi.org/10.1016/j.matchar.2003.09.001

[3] M. Persyk, A.W. Kochański, Prediction of ductile cast iron quality by artificial neural networks, Journal of Materials Research and Technology, 109 (2001) 305-307. https://doi.org/10.1016/S0924-0136(00)00822-0

[4] E. Fraś, M. Górny, H. Lopez, Thin wall ductile iron castings as substitutes for aluminium alloy casting, Archives of Metallurgy and Materials, 59 (2) (2014) 459-465. https://doi.org/10.2478/amm-2014-0076

[5] G. Rivera, R. Boeri, J. Sikora, Influence of the solidification microstructure on the mechanical properties of ductile iron, International Journal of Cast Metal Research, 11 (6) (1999) 533-538. https://doi.org/10.1080/13640461.1999.11819329

[6] J.W. Soedarsono, T.P. Soemardi, B. Suharno, R.D. Sulamet-Ariobimo, Effects of carbon equivalent on the microstructures of thin wall ductile iron, Journal of Materials Science and Engineering, 5 (2011) 266-270

[7] M. Ghoroghi, N. Varahram, Y. Perseh, Investigation into microstructure and mechanical properties of heavy section nickel alloyed austempered ductile iron in accordance with austempering parameters, Material Design & Processing Communications, 3 (4) (2021) 5-11. https://doi.org/10.1002/mdp2.220

[8] J. Lacaze, S. Armendariz, P. Larrañaga, I. Asenjo, J. Sertucha, R. Suárez, Effect of carbon equivalent on graphite formation in heavy-section ductile iron parts, Materials Science Forum, 636-637 (2010) 523–530. https://doi.org/10.4028/www.scientific.net/MSF.636-637.523

[9] R.A. Martínez, R.E. Boeri, J.A. Sikora, Application of ADI in high strength thin wall automotive parts, 2002 World Conference on ADI, September 26-27, Kentucky, USA, 2002, 143-148.

[10] B.I. Imasogie, U. Wendt, Characterization of graphite particle shape in spheroidal graphite iron using a computer-based image analyzer, Journal of Minerals & Materials Characterization & Engineering, 3 (1) (2004) 1-12. https://doi.org/10.4236/jmmce.2004.31001

[11] K. Davut, B. Çetin, E. Arslan, H. Meco, C. Yazganarikan, Nodularity and nodule count analysis of austempered ductile iron castings by digital image processing, 18th International Metallurgy and Materials Congress, 29 Sept-01 Oct, Istambul, Turkey, 2016, 497-500.

[12] G. Das, Image analysis in quantitative metallography, Materials Characterization Techniques-Principles and Applications, 83 (1007) (1999) 135-150.

[13] C.A. Paredes-Orta, F. Manriquez-Guerrero, J. Torres-González, F. Castañeda, I.R. Terol-Villalobos, Wear characterization of nodular cast iron based on clusters

of nodules, Advanced Materials Research, 976 (2014) 184–188. https://doi.org/10.4028/www.scientific.net/AMR.976.184

[14] E. Colin García, A. Cruz Ramírez, G. Reyes Castellanos, J. Téllez Ramírez, A. Magaña Hernández, Microstructural and mechanical assessment of camshafts produced by ductile cast iron low alloyed with vanadium, Metals, 11 (146) (2021) 1–18. https://doi.org/10.3390/met11010146

[15] M. Górny, M. Kawalec, B. Gracz, M. Tupaj, Influence of cooling rate on microstructure formation of Si–Mo ductile iron castings, Metals, 11 (1634) (2021) 1-15. https://doi.org/10.3390/met11101634

[16] H. Ma, R.J. Bowers, D.O. Northwood, X. Sun, P.J. Bauerle, Residual stress and retained austenite in induction hardened ductile iron camshafts, WIT Transactions on Engineering Sciences, 76 (2012) 115–127. https://doi.org/10.2495/TD120101

[17] Riposan, D. Anca, I. Stan, M. Chisamera, S. Stan, Graphite nodularity evaluation in high-Si ductile cast irons, Materials, 15 (7685) (2022) 1-21. https://doi.org/10.3390/ma15217685

[18] A.D. Sosa, M.D. Echeverría, O.J. Moncada, N. Míngolo, J.A. Sikora, Influence of nodule count on residual stresses and distortion in thin wall ductile iron plates of different matrices, Journal of Materials Processing Technology, 209 (15-16) (2009) 5545–5551. https://doi.org/10.1016/j.jmatprotec.2009.05.010

[19] E. Colin-García, A. Cruz-Ramírez, G. Reyes-Castellanos, J.A. Romero-Serrano, R.G. Sánchez-Alvarado, M. Hernández-Chávez, Influence of nickel addition and casting modulus on the properties of hypo-eutectic ductile cast iron, Journal of Mining and Metallurgy, Section B: Metallurgy, 55 (2) (2019) 283–293. https://doi.org/10.2298/JMMB181012023C

[20] H. Sazegaran, F. Teimoori, H. Rastegarian, A.M. Naserian-Nik, Effects of aluminum and copper on the graphite morphology, microstructure, and compressive properties of ductile iron, Journal of Mining and Metallurgy, Section B: Metallurgy, 27 (1) (2021) 145–154. https://doi.org/10.2298/JMMB191224006S

[21] C. Chuang, D. Singh, P. Kenesei, J. Almer, J. Hryn, R. Huff, 3D quantitative analysis of graphite morphology in high strength cast iron by high-energy X-ray tomography, Scripta Materialia, 106 (2015) 5–8. https://doi.org/10.1016/j.scriptamat.2015.03.017

[22] L.A. Morales-Hernández, I.R. Terol-Villalobos, A. Domínguez-González, F. Manríquez-Guerrero, G. Herrera-Ruiz, Spatial distribution and spheroidicity characterization of graphite nodules based on morphological tools, Journal of Materials Processing Technology, 210 (2) (2010) 335–342. https://doi.org/10.1016/j.jmatprotec.2009.09.020

[23] Foseco Ferrous Foundryman´s handbook, Butterworth Heinemann, Oxford, 2000, 32-34.

[24] Ch.F. Han, Y.F. Sun, Y. Wu, Y.H. Ma, Effects of vanadium and austempering temperature on microstructure and properties of CADI, Metallography, Microstructure, and Analysis, 4 (2015) 135–145. https://doi.org/10.1007/s13632-015-0197-1

[25] R.E. Ruxanda, D.M. Stefanescu, T.S. Piwonka, Microstructure characterization of ductile thin-wall iron castings, AFS Transaction, 110 (2002) 1-17.

[26] S.K. Putatunda, Influence of austempering temperature on microstructure and fracture toughness of a high-carbon, high-silicon and high-manganese cast steel, Materials & Design, 24 (6) (2003) 435–443. https://doi.org/10.1016/S0261-3069(03)00090-6

[27] L. Rao, W.W Tao, S.J. Wang, M.P. Geng, G.X. Cheng, Influence of the composition ratio of manganese and copper on the mechanical properties and the machining performance of ductile iron, Indian Journal of Engineering and Materials Sciences, 21 (5) (2014) 573-579.

[28] S. Dhanasekaran, A. Vadiraj, G. Balachandran, M. Kamaraj, Mechanical behavior of an austempered ductile iron, Transactions of The Indian Institute of Metals, 63 (2010) 779-785. https://doi.org/10.1007/s12666-010-0119-5

[29] A.S. Darmawan P.I. Purboputro, A. Yulianto, A.D. Anggono, W. Wijianto, M. Masyrukan, R.D. Setiawan, N.D. Kartika, Effect of magnesium on the strength, stiffness and toughness of nodular cast iron, Materials Science Forum, 991 (2020) 17–23. https://doi.org/10.4028/www.scientific.net/MSF.991.17

[30] G.M. Goodrich, Cast iron microstructure anomalies and their causes, AFS Transactions, 105 (1997) 669–683.

[31] N. Fatahalla, H. Abd Al Hakim, A. Abo-El-Ezz, M. Mohamed, Effect of the percentage carbon equivalent on the nodule characteristics, density and modulus of elasticity of ductile cast iron, Journal of Materials Science, 31 (18) (1996) 4933–4937. https://doi.org/10.1007/BF00355883

[32] E. Moumeni, C.C. Tutum, N.S. Tiedje, J. H. Hattel, Analysis of nucleation modelling in ductile cast iron, IOP Conference Series: Materials Science and Engineering, January 01, Aachen, 2011. 1-7. https://doi.org/10.1088/1757-899X/27/1/012062

[33] D.I. Pedro, R.C. Dommarco, Rolling contact fatigue resistance of carbidic austempered ductile iron (CADI), Wear, 418–419 (2018) 94–101. https://doi.org/10.1016/j.wear.2018.11.005

[34] A.M. Herrera Navarro, H. Jiménez Hernández, H. Peregrina-Barreto, F. Manríquez Guerrero, I.R. Terol Villalobos, Characterization of the roundness degree of graphite nodules in ductile iron a new discrete measure independent to resolution, Superficies y vacío, 26 (2) (2013) 58-63.

[35] Mr. Bahubali, B. Sangame, M. Vasudev, D. Shinde, The effect of inoculation on microstructure and mechanical properties of ductile iron, Journal of Mechanical and Civil Engineering, 5 (6) (2013) 17-23.

[36] R. Lora, A. Diószegi, L. Elmquist, Solidification study of gray cast iron in a resistance furnace, Key Engineering Materials, 547 (2011) 108–113. https://doi.org/10.4028/www.scientific.net/KEM.457.108

[37] N.G. Kok Long, H. Sasaki, H. Kimura, T. Yoshikawa, M. Maeda, Heterogeneous nucleation of graphite on rare earth compounds during solidification of cast iron, ISIJ International, 58 (1) (2018) 123–131. https://doi.org/10.2355/isijinternational.ISIJINT-2017-398

[38] A. de Albuquerque Vicente, J.R. Sartori Moreno, T.F. de Abreu Santos, D.C. Romano Espinosa, J.A. Soares Tenório, Nucleation and growth of graphite particles in ductile cast iron, Journal of Alloys and Compounds, 775 (2019) 1230–1234. https://doi.org/10.1016/j.jallcom.2018.10.136

[39] M. Górny, E. Tyrała, Effect of cooling rate on microstructure and mechanical properties of thin-walled ductile iron castings, Journal of Materials Engineering and Performance, 22 (2013) 300–305. https://doi.org/10.1007/s11665-012-0233-0

[40] R. Salazar, M. Herrera-Trejo, M. Castro, J. Méndez, J. Torres, M. Méndez, Effect of nodule count and cooling rate on as-cast matrix of a Cu-Mo spheroidal graphite, Journal of Materials Engineering and Performance, 8 (1999) 325-329. https://doi.org/10.1361/105994999770346873

[41] A. Sadjghzadeh Benam, Effect of alloying elements on austempered ductile iron (ADI) properties and its process: Review, China Foundry, 12 (1) (2015) 54–70.

[42] P. Sellamuthu, D.G. Harris Samuel, D. Dinakaran, V.P. Premkumar, Z. Li, S. Seetharaman, Effect of nickel content and austempering temperature on microstructure and mechanical properties of austempered ductile iron (ADI), IOP Conference Series: Materials Science and Engineering, February 24-26, Bangkok, Thailand. 2018, 1–7. https://doi.org/10.1088/1757-899X/383/1/012069

[43] K.M. Pedersen N. Tiedje, Solidification of hypereutectic thin wall ductile cast iron, Materials Science Forum, 508 (2006) 63–68. https://doi.org/10.4028/www.scientific.net/MSF.508.63

[44] S.C. Murcia, E.A. Ossa, D. J. Celentano, Nodule evolution of ductile cast iron during solidification, Metallurgical and Materials Transactions B: Process Metallurgy and Materials Processing Science, 45 (2014) 707–718. https://doi.org/10.1007/s11663-013-9979-5

[45] M. Bjerre, N.S. Tiedje, J. Thorborg, J.H. Hattel, Modelling the solidification of ductile cast iron parts with varying wall thicknesses, IOP Conference Series: Materials Science and Engineering June 21-26, Hyogo, Japan, 2015, 1-8. https://doi.org/10.1088/1757-899X/84/1/012038

[46] O.A. Tchaykovsky, O.V. Klok, Ductile cast iron induction Re-Melting, International Journal of Engineering Research & Technology (IJERT), 4 (7) (2015) 836-841.

[47] A. Vaško, Evaluation of shape of graphite particles in cast irons by a shape factor, Materials Today: Proceedings, 3 (4) (2016) 1199-1204. https://doi.org/10.1016/j.matpr.2016.03.006

[48] R.E.L. Ruxunda, D.M. Stefanescu, T.S. Piwonka, Quantification of the solidification microstructure of ductile iron through Image analysis, Proceedings of the International Conference on the Science of Casting and Solidification, January, Brasov, Romania, 2001, 361-368.

[49] J.M. Bojarro, R.A. Martínez, R.E. Boeri, J.A. Sikora, Shape and count of free graphite particles in thin wall ductile iron castings, ISIJ International, 42 (3) (2002) 257-263. https://doi.org/10.2355/isijinternational.42.257

[50] S. Toraman, T. Cosgun, B. Alkan, B. Cetin, O. Akyildiz, Assessing the volume fractions of the phases, nodularity and nodule count of spheroidal graphite cast iron using Image j software, Mugla Journal of Science and Technology, 5 (1) (2019) 137–142. https://doi.org/10.22531/muglajsci.521128

[51] P.H. Agarwal, M. Mamta, P. Patel, Effect of magnesium as spherodizer on graphite morphology in ductile cast iron, International Journal of Advance Engineering and Research Development, 3 (2) (2016) 60-63.

[52] M. Holtzer, M. Górny, R. Dańko, Microstructure and properties of ductile iron and compacted graphite iron castings, Springer Cham, Heidelberg, New York, Dordrecht, London, 2015, 109-121

[53] Jh. Liu, Js. Yan, Xb. Zhao, Bg. Fu, Ht. Xue, Gx. Zhang, Ph. Yang, Precipitation and evolution of nodular graphite during solidification process of ductile iron, China Foundry, 17 (4) (2020) 260–271. https://doi.org/10.1007/s41230-020-0042-2

[54] M. Riebisch, B. Pustal, A. Bührig-Polaczek, Influence of carbide-promoting elements on the microstructure of high-silicon ductile iron, International Journal of Metalcasting, (14) (2020) 1152–1161. https://doi.org/10.1007/s40962-020-00442-1

[55] G.F. Vander Voort, Metallography Principles and practice, ASM International, USA, 1999, 411-414.

[56] E. Ghassemali, J.C. Hernando, D.M. Stefanescu, A. Doiszegi, A.E.W. Jarfors, J. Dluhos, M. Petrenec, Revisiting the graphite nodule in ductile iron, Scripta Materialia, 161 (2019) 66–69. https://doi.org/10.1016/j.scriptamat.2018.10.018

[57] K.L. Hayrynen, The production of austempered ductile iron (ADI), 2002 World Conference on ADI, September 26-27, Kentucky, USA, 2002, 1-6.

[58] W.C. Johnson, B.V Kovacs, The effect of additives on the eutectoid transformation of ductile iron, Metallurgical Transactions A, 9 (1976) 219-229. https://doi.org/10.1007/BF02646704

[59] J. Lacaze, J. Sertucha, L. Magnusson Åberg, Microstructure of as-cast ferritic-pearlitic nodular cast irons, ISIJ International, 56 (9) (2016) 1606–1615. https://doi.org/10.2355/isijinternational.ISIJINT-2016-108

[60] W. Arshad, A. Mehmood, M.F. Hashmi, O.U. Rauf, The effect of increasing silicon on mechanical properties of ductile iron, Journal of Physics: Conference Series, 1082 (2018) 1-6. https://doi.org/10.1088/1742-6596/1082/1/012059

[61] R.A. Gonzaga, Influence of ferrite and pearlite content on mechanical properties of ductile cast irons, Materials Science and Engineering: A, 567 (2013) 1–8. https://doi.org/10.1016/j.msea.2012.12.089

[62] A. Javaid, J. Thomson, M. Sahoo, K.G. Davis, Factors affecting the formation of carbides in thin wall DI castings, AFS transactions, 74 (1999) 441-456.

[63] M. Caldera, G.L. Rivera, R.E. Boeri, J.A. Sikora, Precipitation and dissolution of carbides in low alloy ductile iron plates of varied thickness, Materials Science and Technology, 21 (10) (2005) 1187–1191. https://doi.org/10.1179/174328405X62242

[64] M. Rezvani, R. A. Harding, J. Campbell, The effect of vanadium in as-cast ductile iron, International Journal of Cast Metals Research, 10 (1) (1997) 1–15. https://doi.org/10.1080/13640461.1997.11819213

[65] I. Minkoff, Alloy cast iron systems, The physical metallurgy of cast iron, Jhon Wiley and Sons Ltd., Norwich, England, 1983, 185-188.

[66] A. Cruz Ramírez, E. Colin García, J.F. Chávez Alcalá, J. Téllez Ramírez, A. Magaña Hernández, Evaluation of CADI low alloyed with chromium for camshafts application, Metals, 12 (249) (2022) 1-24. https://doi.org/10.3390/met12020249

[67] W.D. Callister Jr, Materials science and engineering an

Introduction, John Wiley and Sons Ltd., USA, 2007, 291.

[68] E. Guzel, C. Yuksel, Y. Bayrak, O. Sen, A. Ekerim, Effect of section thickness on the microstructure and hardness of ductile cast iron, Metallography and Hardness Measurements, 56 (4) (2014) 285–288. https://doi.org/10.3139/120.110558

[69] J.M. Radzikowska, Effect of specimen preparation on evaluation of cast iron microstructures, Materials Characterization, 54 (4-5) (2005) 287–304. https://doi.org/10.1016/j.matchar.2004.08.019

UTICAJ REGULARNE DEBLJINE NA MIKROSTRUKTURNU I KVANTITATIVNU ANALIZU HIPOEUTEKTIČKOG DUKTILNOG GVOŽĐA LEGIRANOG SA Ni I V

E. Colin-García [a,*], R.G. Sánchez-Alvarado [a], A. Cruz-Ramírez [b], M.A. Suarez-Rosales [c], L. Portuguez-Pardo [a], J.C. Jiménez-Lugos [a]

[a] Nacionalni politehnički institut – ESIQIE, Odeljenje za metalurgiju i inženjerstvo materijala, Meksiko Siti, Meksiko

[b] Nacionalni politehnički institut – UPIIH, Odeljenje za osnovne nauke, Idalgo, Meksiko

[c] Autonomni univerzitet Metropolitan – UAM-Askapotzalko, Odeljenje za materijale, Meksiko Siti, Meksiko

Apstrakt

Duktilno gvožđe sadrži slobodne grafitne nodule unutar metalne matrice, koja se uglavnom sastoji od ferita i perlita u livenom stanju. Debljina odlivaka ima veliki uticaj na veličinu, oblik i količinu mikrokomponenti metalne matrice i grafitnih nodula, a time i na mehanička svojstva. U ovoj studiji ispitivana je brzina hlađenja (prouzrokovana debljinom odlivaka) na metalnoj matrici i sferna svojstva niskolegiranog duktilnog gvožđa sa 0,8 %Ni i 0,15 %V. Duktilno gvožđe je proizvedeno u sendvič procesu sa inokulacijom lopaticom. U kalupu od sirovog peska proizvedeno je šest ploča različite debljine, od 4,3 mm do 25,4 mm. Mikrostrukturna karakterizacija je izvršena optičkom mikroskopijom (OM), skenirajućom elektronskom mikroskopijom (SEM) i softverom Image J korišćenjem različitih metoda kvantifikacije. Metoda površine za određivanje prosečne veličine nodula i strukture nodula dala je pouzdanije rezultate od metoda perimetra i ukupnog broja čestica. Za mehaničku karakterizaciju korišćen je test tvrdoće na Rockvell C skali. Nizak sadržaj vanadijuma koji je dodat duktilnom livenom gvožđu imao je zanemarljiv uticaj na obrazac očvršćavanja, što je uglavnom bilo zbog efekta formiranja grafita dodatka nikla i silicijuma. Rezultati mikrostrukturnih karakteristika su ovakvi prvenstveno zbog brzine hlađenja, koja je određena debljinom odlivaka. Najtanja livena ploča značajno je poboljšala broj nodula (414 Nod/mm^2), sferičnost (0,96) i nodularnost (96,21 %). Nasuprot tome, najdeblja ploča za livenje postigla je najveći zapreminski udeo grafita (10,85 %) i najmanji zapreminski udeo neželjenih čestica (0,36 %). Visoka brzina hlađenja najtanje ploče za livenje rezultirala je najvećom tvrdoćom od 31,56 HRC zbog većeg zapreminskog udela perlita (33,7 %) i karbida (4,5 %).

Ključne reči: *Duktilno gvožđe; Debljina; Mikrostruktura; Brzina hlađenja; Kvantitativna analiza; Nodularne karakteristike*